

1
2
3
4
5
6
7
8
9
10
11
12
13
14
15
16
17

Stringent and complex sequence constraints of an IGHV1-69 broadly neutralizing antibody to influenza HA stem

Qi Wen Teo^{1,2,*}, Yiquan Wang^{1,*}, Huibin Lv^{1,2,*}, Timothy J.C. Tan³, Ruipeng Lei¹, Kevin J. Mao¹,
Nicholas C. Wu^{1,2,3,4,§}

¹ Department of Biochemistry, University of Illinois Urbana-Champaign, Urbana, IL 61801, USA

² Carl R. Woese Institute for Genomic Biology, University of Illinois Urbana-Champaign, Urbana, IL 61801, USA

³ Center for Biophysics and Quantitative Biology, University of Illinois Urbana-Champaign, Urbana, IL 61801, USA

⁴ Carle Illinois College of Medicine, University of Illinois Urbana-Champaign, Urbana, IL 61801, USA

* These authors contributed equally to this work

§ To whom correspondence may be addressed. Email: nicwu@illinois.edu (N.C.W.)

18 **ABSTRACT**

19 IGHV1-69 is frequently utilized by broadly neutralizing influenza antibodies to the hemagglutinin
20 (HA) stem. These IGHV1-69 HA stem antibodies have diverse complementarity-determining
21 region (CDR) H3 sequences. Besides, their light chains have minimal to no contact with the
22 epitope. Consequently, sequence determinants that confer IGHV1-69 antibodies with HA stem
23 specificity remain largely elusive. Using high-throughput experiments, this study revealed the
24 importance of light chain sequence for the IGHV1-69 HA stem antibody CR9114, which is the
25 broadest influenza antibody known to date. Moreover, we demonstrated that the CDR H3
26 sequences from many other IGHV1-69 antibodies, including those to HA stem, were
27 incompatible with CR9114. Along with mutagenesis and structural analysis, our results indicate
28 that light chain and CDR H3 sequences coordinately determine the HA stem specificity of
29 IGHV1-69 antibodies. Overall, this work provides molecular insights into broadly neutralizing
30 antibody responses to influenza virus, which have important implications for universal influenza
31 vaccine development.

32 INTRODUCTION

33 Influenza viruses pose a constant threat to public health, resulting in substantial morbidity and
34 mortality with approximately 500,000 deaths worldwide each year.¹ Although vaccination
35 remains the foremost measure for preventing and controlling influenza virus infection, the
36 effectiveness of the annual seasonal influenza vaccine has varied widely, ranging from 19% to
37 60% over the past decade.² This variability is largely due to the continuous antigenic drift of
38 human influenza virus, especially at the immunodominant head domain of hemagglutinin (HA),
39 which can in turn lead to vaccine mismatch in some influenza seasons.^{3,4} In addition, the current
40 seasonal influenza vaccine is designed to protect against influenza A H1N1 and H3N2 subtypes,
41 as well as influenza B virus, but not avian influenza A subtypes with zoonotic potential, such as
42 H5N1 and H7N9. Therefore, significant efforts have been made to develop a universal influenza
43 vaccine that targets the highly conserved HA stem domain,^{5,6} with an ultimate goal to elicit
44 broadly neutralizing HA stem antibodies like CR9114, which can bind to both group 1 (e.g. H1
45 and H5) and group 2 (e.g. H3 and H7) HAs as well as influenza B HAs.⁷

46
47 Many HA stem antibodies, including CR9114, are encoded by IGHV1-69.⁸⁻¹⁰ Structural analyses
48 have shown that the paratopes of these IGHV1-69 antibodies are dominated by the heavy chain
49 with minimal to no contribution from the light chain.^{7,11-13} Consistently, diverse light chain
50 germline genes are found among IGHV1-69 HA stem antibodies (e.g. IGKV1-44,⁷ IGLV1-51,^{9,12}
51 IGLV10-54,¹¹ and IGKV3-20¹³). Similarly, the complementarity-determining region (CDR) H3
52 sequences, which are formed by VDJ recombination, are highly diverse among IGHV1-69 HA
53 stem antibodies.¹⁴ Although most IGHV1-69 HA stem antibodies encode a Tyr in the CDR H3,
54 the position of this Tyr varies, and some do not even have a Tyr in the CDR H3.¹⁴ Based on
55 these observations, IGHV1-69 HA stem antibodies do not seem to have strong sequence
56 preferences in the CDR H3 and light chain. At the same time, it is impossible that all IGHV1-69
57 antibodies can bind to HA stem, given that many IGHV1-69 antibodies are specific to other

58 pathogens.¹⁵ Besides, some IGHV1-69 antibodies bind to HA head instead of HA stem.^{16,17}
59 Therefore, despite the first IGHV1-69 HA stem antibody being discovered 15 years ago,⁹ it
60 remains unclear what sequence features make an IGHV1-69 antibody bind to the HA stem.

61
62 In this study, we performed two high-throughput experiments to probe the sequence constraints
63 in the light chain and CDR H3 of the IGHV1-69 HA stem antibody CR9114, which is the
64 broadest influenza neutralizing antibody known to date.⁷ Our first high-throughput experiment
65 examined the compatibility of 78 light chain sequences from diverse IGHV1-69 antibodies with
66 CR9114 heavy chain. Our findings indicated that despite having no contact with the HA stem
67 epitope, light chain of CR9114 contained sequence determinants for its binding activity.
68 Specifically, we demonstrated that the amino acid sequences at V_L residues 91 and 96 hugely
69 influenced the light chain compatibility with CR9114 heavy chain for binding to HA stem. Of note,
70 the Kabat numbering scheme is used throughout. Our second high-throughput experiment
71 measured the binding affinity of 2,162 diverse CDR H3 variants to HA stem and showed that
72 most CDR H3 variants, including many from other IGHV1-69 HA stem antibodies, were
73 incompatible with CR9114. These results indicate that the sequence constraints in the CDR H3
74 and light chain of IGHV1-69 HA stem antibodies are stringent yet complex.

75

76 **RESULTS**

77 **Light chain sequence of CR9114 is important for HA stem binding**

78 A previous structural study has shown that CR9114, which is encoded by IGHV1-69 and IGLV1-
79 44, does not use light chain for binding (**Figure 1A**).⁷ In addition, the HA stem binding activity of
80 CR9114 is not affected by replacing its light chain by one from an antibody of different
81 specificity.¹⁰ Here, we aimed to systematically investigate if the sequence of CR9114 light chain
82 is truly unimportant for HA stem binding. Briefly, we compiled a list of 120 antibodies from
83 Genbank that are encoded by IGHV1-69 with different λ light chains (**Table S1**). The light chain

84 sequences from these 120 antibodies were synthesized and paired with the germline sequence
85 of CR9114 heavy chain to create a light chain variant library. We also included 10 light chain
86 sequences with premature stop codons as negative controls. As a result, our light chain variant
87 library contained 130 different light chain sequences, all of which paired with the germline
88 sequence of CR9114 heavy chain. Of note, the germline sequence of CR9114 heavy chain was
89 used because we wanted to avoid any incompatibility between heavy chain somatic
90 hypermutations and light chain variants.

91
92 Subsequently, this light chain variant library was displayed on the yeast cell surface, and two-
93 way sorted based on antibody expression level as well as binding activity to mini-HA, which is a
94 trimeric HA stem construct without the head domain (**Figure 1B**).⁵ Four sorted populations were
95 collected, namely no expression, high expression, no binding, and high binding. The frequency
96 of each light chain variant in each sorted population was quantified by next-generation
97 sequencing. Among the 130 light chain variants in the library, 78 had an average occurrence
98 frequency of >0.2% across different sorted populations and were subjected to downstream
99 analyses (**Table S1**). These 78 light chain variants include the one from CR9114 (i.e., wild type;
100 WT), 13 from other influenza antibodies, 55 from non-influenza antibodies, and 9 negative
101 controls with premature stop codons. For each light chain variant, an expression score and a
102 binding score were computed based on its frequency in different sorted populations (**see**
103 **Methods**). Both the expression and binding scores were normalized such that the scores for
104 WT equaled 1 and the mean scores for negative controls (i.e., variants with stop codons)
105 equaled 0. Pearson correlation coefficients of 0.75 and 0.74 were obtained between two
106 replicates of the binding and expression sorts, respectively (**Figure S1**), confirming the
107 reproducibility of our results.

108

109 Except for the negative controls, most light chain variants had an expression score of around 1
110 (**Figure 1C**), indicating that the light chain sequence of CR9114 germline had minimal influence
111 on expression. However, many light chain variants had a low binding score (**Figure 1C**). In
112 addition, the binding scores of light chain variants from influenza antibodies (mean = 0.84) were
113 significantly higher than those from non-influenza antibodies (mean = 0.49, p-value = 0.005,
114 two-tailed Student's t-test), despite having similar expression scores (mean = 1.03 and 0.99,
115 respectively, p-value = 0.35, two-tailed Student's t-test). These results imply that the light chain
116 sequence of CR9114 germline is an important determinant for its HA stem binding activity.

117

118 **Importance of CR9114 light chain residues 91 and 96**

119 Next, we aimed to understand the molecular mechanism of how light chain modulated the HA
120 stem binding activity of CR9114 germline. Since CR9114 light chain has no contact with the HA
121 stem epitope (**Figure 1A**),⁷ its sequence determinants likely locates at the heavy-light chain
122 interface. Structural analysis of the previously determined crystal structure of CR9114 in
123 complex with HA⁷ suggested that V_L residues 91 and 96 in CDR L3 are critical for stabilizing the
124 conformation of CDR H3, which in turn is important for binding (**Figure 2A**). CR9114 has an
125 aromatic residue Trp at V_L residue 91, which forms an extensive π - π stacking network with four
126 aromatic residues in CDR H3, namely V_H Y98, V_H Y99, V_H Y100, and V_H Y100a, as well as V_H
127 W47 in the heavy chain framework region 2. In contrast, CR9114 has a small amino acid Ala at
128 V_L residue 96, which points toward the heavy chain with limited space in between. These
129 observations suggested that the compatibility of different light chain variants and CR9114
130 germline heavy chain depended on the amino acid identities at V_L residues 91 and 96.
131 Specifically, we hypothesized that amino acids F/Y/W, which are both aromatic and bulky, were
132 required at V_L residue 91 but forbidden at V_L residue 96.

133

134 We then compared the amino acid sequences at V_L residues 91 and 96 between high-binding
135 and low-binding light chain variants, using an arbitrary binding score cutoff of 0.8 (**Figure 2B**).
136 At V_L residue 91, all light chain variants with a binding score >0.8 contained an aromatic amino
137 acid (i.e., W/Y/F), whereas non-aromatic amino acids could be observed among variants with a
138 binding score <0.8. Conversely, aromatic amino acids were enriched at V_L residue 96 among
139 variants with a binding score <0.8. These observations are consistent with our hypothesis above.

140

141 To further experimentally validate our findings, we introduced different mutations at residues 91
142 and 96 of CR9114 light chain, recombinantly expressed them by pairing with CR9114 germline
143 heavy chain, and then tested their binding affinity to mini-HA. Hereafter, CR9114 with germline
144 heavy chain is abbreviated as CR9114 gHC. The binding activity of CR9114 gHC to mini-HA
145 was abolished by substituting V_L W91 with non-aromatic amino acids T/R/A, but not aromatic
146 amino acids Y/F (**Table 1 and Figure S2**). Likewise, the binding activity of CR9114 gHC to mini-
147 HA was abolished by substituting V_L A96 with aromatic amino acids W/F, but not non-aromatic
148 amino acids V/S/R (**Table 1 and Figure S2**). Therefore, our binding experiment confirms that V_L
149 residues 91 and 96 in the CDR L3 are important for CR9114 to interact with the HA stem,
150 despite not being part of the paratope.

151

152 **Additional sequence constraints in CR9114 light chain**

153 Although our results indicated that aromatic amino acids were required at V_L residue 91 but
154 forbidden at V_L residue 96 of CR9114, exceptions existed in our light chain variant library (**Table**
155 **S1**). Specifically, we noticed that some light chain variants with a low binding score had
156 aromatic (i.e., F/Y/W) and non-aromatic amino acids (i.e., non-F/Y/W) at V_L residues 91 and 96,
157 respectively (i.e., V_L 91_{F/Y/W}/96_{non-F/Y/W}). This observation suggests that there are additional
158 sequence constraints in the light chain of CR9114.

159

160 Members of our light chain variant library were from three IGLV families, namely IGLV1, IGLV2,
161 and IGLV3. For light chain variants in IGLV1 family, those with $V_L 91_{F/Y/W}/96_{non-F/Y/W}$ had
162 significantly higher binding scores than those without (p-value = $2e-4$, two-tailed Student's t-test,
163 **Figure 2C**). In contrast, while the light chain variants in IGLV2 family with $V_L 91_{F/Y/W}/96_{non-F/Y/W}$
164 also had higher binding scores than those without, such difference was not as significant (p-
165 value = 0.10, two-tailed Student's t-test, **Figure 2C**). Furthermore, the binding scores of light
166 chain variants in IGLV3 family with and without the $V_L 91_{F/Y/W}/96_{non-F/Y/W}$ motif had no significant
167 difference (p-value = 0.94, two-tailed Student's t-test) and were generally low (**Figure 2C**). Of
168 note, in all three IGLV families, the expression scores of light chain variants with and without V_L
169 $91_{F/Y/W}/96_{non-F/Y/W}$ had no significant difference (p-values ranging from 0.31 to 0.84, two-tailed
170 Student's t-test, **Figure S3A**). These results show that besides the amino acid sequences at V_L
171 residues 91 and 96, sequence differences among IGLV families could also influence the binding
172 activity of CR9114 to HA stem.

173
174 Our additional analysis suggested that a CDR L3 length of 11 was optimal for CR9114 binding
175 to the HA stem (**Figure S3B**), since the binding scores of light chain variants lowered when the
176 CDR L3 lengths deviated from 11. In contrast, the expression scores were similar across light
177 chain variants with different CDR L3 lengths (**Figure S3C**). We also analyzed the relationship
178 between binding scores and the number of V_L somatic hypermutations (SHMs), but no
179 significant correlation was found (p-values ranging from 0.39 to 0.98, Pearson correlation test,
180 **Figure S3D-F**). Overall, our analyses demonstrate that light chain germline features, including
181 CDR L3 length and germline gene usage, are important sequence determinants for the HA stem
182 binding activity of CR9114.

183

184 **High-throughput characterization of CDR H3 variants**

185 Similar to the light chain, the sequence constraints of the CDR H3 of IGHV1-69 HA stem
186 antibodies have also been unclear, especially since they are highly diverse.¹⁴ Therefore, we
187 next aimed to probe the sequence constraints of CR9114 CDR H3. Briefly, we compiled a list of
188 3,325 CDR H3 sequences from diverse IGHV1-69 antibodies from Genbank (**Table S2**).
189 Additionally, we performed a site-saturation mutagenesis of the CDR H3 of CR9114. Together
190 with the WT CDR H3 sequence of CR9114, a CDR H3 library with 3,606 variants in CR9114
191 gHC was constructed and displayed on yeast cell surface. Tite-Seq¹⁸ was then applied to
192 measure the apparent dissociation constant (K_D) values of individual variants to mini-HA (**Figure**
193 **3A**). At the same time, antibody expression level was measured by two-way cell sorting and
194 next-generation sequencing, as described above for the light chain variant library. The
195 expression score for each CDR H3 variant was normalized such that the score for WT equaled
196 1 and the mean score for nonsense mutants of CR9114 CDR H3 equaled 0.

197
198 After filtering out CDR H3 variants with low occurrence frequency or noisy estimation in the
199 apparent K_D values (**see Methods**), 2,162 CDR H3 variants were subjected to downstream
200 analyses (**Table S2**). These included the WT CDR H3 of CR9114, 206 single amino acid
201 mutants of CR9114 CDR H3, 14 nonsense mutants of CR9114 CDR H3, 73 CDR H3 variants
202 from HA stem antibodies, 245 from non-HA stem influenza antibodies, and 1,623 from non-
203 influenza antibodies. Pearson correlations of 0.71 and 0.61 were obtained between two
204 replicates of Tite-Seq and expression sort, respectively (**Figure S4A-B**), confirming the
205 reproducibility of our results. As expected, the expression score of nonsense mutants of
206 CR9114 CDR H3 was significantly lower than other CDR H3 variants (p -values = $2e-22$ to $1e-47$,
207 two-tailed Student's t -test, **Figure S4D**). Similarly, the binding affinity of nonsense mutants of
208 CR9114 CDR H3 to mini-HA was significantly weaker than that of single amino acid mutants of
209 CR9114 CDR H3 (p -value = $1e-17$, two-tailed Student's t -test, **Figure 3B-C**). These results
210 validated the quality of our data.

211

212 **Most CDR H3 variants are incompatible with CR9114 for HA stem binding**

213 While the apparent K_D values of many single amino acid mutants of CR9114 CDR H3 to mini-
214 HA were around 1 nM, those of CDR H3 variants from other antibodies, including HA stem
215 antibodies, were mostly between 100 nM to 1 μ M (**Figure 3B-C**). In contrast, the expression
216 scores of single amino acid mutants of CR9114 CDR H3 and other CDR H3 variants were
217 similar (p -values = 0.22 to 0.76, two-tailed Student's t -test, **Figure S4D**). Of note, several CDR
218 H3 variants from non-influenza antibodies had an apparent K_D of around 1 nM (**Figure S4C and**
219 **Table S2**). However, when we recombinantly expressed one of these CDR H3 variants, it did
220 not show binding to mini-HA, indicating there were false positives in our Tite-Seq experiment
221 (**Figure S4E**). Together, these observations suggest that the CDR H3 of CR9114 has a
222 stringent sequence requirement for HA stem binding.

223

224 A previous study has demonstrated that many IGHV1-69 HA stem antibodies, including CR9114,
225 are featured by a CDR H3-encoded Tyr at V_H residue 98 that interacts extensively with the HA
226 stem epitope.¹⁴ Consistently, our results showed that CDR H3 variants with Y98 had slightly, yet
227 significantly, better apparent K_D values (p -values = 0.001 to 0.03, two-tailed Student's t -test,
228 **Figure 3D**). In contrast, CDR H3 variants with and without Tyr, regardless of the residue
229 position, did not show any significant difference in apparent K_D values (p -values = 0.20 to 0.91,
230 two-tailed Student's t -test, **Figure 3E**). Therefore, our result substantiates that V_H Y98 partially
231 contributes to the compatibility of CDR H3 variants with CR9114 for HA stem binding. However,
232 given that many CDR H3 variants from IGHV1-69 HA stem antibodies with Y98 are incompatible
233 with CR9114 gHC for binding (**Figure 3D**), the sequence constraints of CR9114 CDR H3 likely
234 involve other CDR H3 residues.

235

236 **Importance of non-paratope residues in CR9114 CDR H3**

237 To further understand the sequence constraints of CR9114 CDR H3, we aimed to identify
238 residues that are key for HA stem binding. Subsequently, we analyzed the single amino acid
239 mutants of CR9114 CDR H3 in our CDR H3 library. Our Tite-Seq result indicated that most
240 mutations at the four consecutive Tyr residues in the CDR H3, namely V_H Y98, V_H Y99, V_H Y100,
241 and V_H Y100a, weakened the binding affinity of CR9114 gHC (**Figure 4A**). This observation is
242 consistent with our structural analysis above (**Figure 2A**), showing that these four Tyr residues
243 form an extensive π - π stacking network with V_H W47 and V_L W91, which is essential for the
244 conformational stability of the CDR H3. Additionally, our Tite-Seq result also revealed the low
245 mutational tolerance of V_H H95 and V_H N97, hence their importance in the HA stem binding
246 activity of CR9114 (**Figure 4A**).

247

248 Based on a previously determined crystal structure of CR9114 in complex with HA,⁷ the side
249 chains of both V_H H95 and V_H N97 are not interacting with the HA stem epitope. Instead, both
250 V_H H95 and V_H N97 form intramolecular interactions to stabilize the CDR H3 conformation. V_H
251 H95 H-bonds with V_H S100b and V_H S35 as well as interacts with V_H Y100 via T-shaped π - π
252 stacking (**Figure 4B**), whereas V_H N97 H-bonds with V_H Y99 and V_H S100b (**Figure 4C**). These
253 observations corroborate our light chain analysis, demonstrating that non-paratope residues that
254 stabilize the CDR H3 conformation are important for the HA stem binding activity of CR9114.

255

256 **DISCUSSION**

257 IGHV1-69 is one of the most highly used heavy chain V genes in the human antibody
258 repertoire,¹⁹ suggesting its importance in the immune system. In fact, many known broadly
259 neutralizing antibodies to various pathogens, such as influenza virus, hepatitis C virus (HCV),
260 and human immunodeficiency virus (HIV), were encoded by IGHV1-69.¹⁵ As a result, IGHV1-69
261 is regarded as an S.O.S. component of the human antibody repertoire.²⁰ However, sequence
262 determinants for the antigen specificity of IGHV1-69 antibodies have been largely elusive. In this

263 study, we used a high-throughput approach to probe the sequence determinants for the HA
264 stem binding activity of CR9114, an IGHV1-69 broadly neutralizing antibody to influenza HA
265 stem.⁷ Our results revealed the importance of the CR9114 light chain in binding, albeit no
266 contact with the epitope. In addition, we showed that the CDR H3 sequence of CR9114 has
267 stringent sequence constraints. Overall, this work advances our understanding of the sequence
268 determinants that define IGHV1-69 HA stem antibodies.

269
270 Our results show that V_L residue 96 in CDR L3 is a determinant for the HA stem binding activity
271 of CR9114. V_L residue 96 in some IGHV1-69 antibodies, including CR9114, is encoded by light
272 chain J gene (**Figure S5A**). Among seven known IGLJ germline genes, three (IGLJ1, IGLJ4,
273 and IGLJ5) encode an aromatic amino acid at V_L residue 96 (**Figure S5B**). Given that aromatic
274 amino acids are forbidden at V_L residue 96 of CR9114, these observations suggest that light
275 chain J gene plays a role in generating IGHV1-69 HA stem antibodies. Of note, the contribution
276 of light chain J gene to antibody binding is rarely reported, if any, since most antibody studies
277 focus on the V genes. However, the sequence determinants for the binding activity of IGHV1-69
278 HA stem antibodies likely vary from antibody to antibody (see discussion below). As a result,
279 additional work is needed to decipher whether light chain J gene usage is a common sequence
280 constraint of IGHV1-69 HA stem antibodies.

281
282 Perhaps the most perplexing result in our study is that most CDR H3 sequences from other
283 IGHV1-69 HA stem antibodies are incompatible with CR9114. Provided that diverse light chain
284 sequences can be observed in IGHV1-69 HA stem antibodies,^{7,9,11-13} the compatibility of a given
285 CDR H3 sequence in IGHV1-69 HA stem antibodies likely depends on their light chain
286 sequences. In other words, we postulate that whether an IGHV1-69 antibody can bind to HA
287 stem is coordinately determined by the light chain and CDR H3 sequences. Consistently, our
288 results revealed the importance of light chain-CDR H3 interaction in the HA stem binding activity

289 of CR9114. Therefore, the sequence determinants of IGHV1-69 HA stem antibodies are
290 stringent yet complex, which explain the lack of sequence convergence among IGHV1-69 HA
291 stem antibodies. Comprehending these sequence determinants will enable an accurate
292 estimation of the proportion of B cells that can give rise to IGHV1-69 HA stem antibodies,
293 especially those that can cross-react to both group 1 and 2 HAs as well as influenza B HA, like
294 CR9114. As the efforts to develop a universal influenza vaccine continue,²¹⁻²³ future studies on
295 the sequence determinants of IGHV1-69 HA stem antibodies are warranted.

296

297 **Limitations of the study**

298 Since our approach has focused on λ light chain of IGHV1-69 antibodies, we were unable to
299 demonstrate whether the κ light chain has similar sequence constraints when paired with
300 CR9114 heavy chain for HA stem binding. Another limitation of our study is that only five
301 antigen concentrations were used in our Tite-Seq experiment as opposed >10 in other Tite-Seq
302 studies.^{18,24,25} This shortcoming would increase the estimation error of apparent K_D values.

303

304 **ACKNOWLEDGEMENTS**

305 This work was supported by the National Institutes of Health R01 AI167910 (N.C.W.), DP2
306 AT011966 (N.C.W.), the Searle Scholars Program (N.C.W.), and Howard Hughes Medical
307 Institute Emerging Pathogens Initiative (N.C.W.).

308

309 **AUTHOR CONTRIBUTIONS**

310 N.C.W. conceived and designed the study. Y.W., H.L., and N.C.W. assembled the dataset.
311 Q.W.T. constructed the yeast libraries and prepared the sequencing libraries. Y.W., and N.C.W.
312 performed data analysis. H.L., T.J.C.T., R.L., and K.J.M. assisted with experiments. Q.W.T.,
313 Y.W., H.L., and N.C.W. wrote the paper and all authors reviewed and/or edited the paper.

314

315 **DECLARATION OF INTERESTS**

316 N.C.W. consults for HeliXon. The authors declare no other competing interests.

317

318 **FIGURE LEGENDS**

319 **Figure 1. Yeast display of light chain variant library with CR9114 germline heavy chain. (A)**

320 Interaction between HA and CR9114 (PDB 4FQI).⁷ Grey: HA1; yellow: HA2; blue: heavy chain;
321 pink: light chain. C_{H1} indicates constant region 1 of heavy chain and C_L indicates constant
322 region 1 of light chain. V_H and V_L indicate variable regions of antibody heavy and light chains,
323 respectively. **(B)** Schematic illustration of measuring the expression level and HA stem binding
324 activity of many light chain variants in parallel using yeast surface display. Briefly, an antibody
325 light chain (LC) variant library was paired with CR9114 germline heavy chain (HC), displayed on
326 the yeast cell surface, and subjected to fluorescence-activated cell sorting (FACS) based on
327 surface expression level and binding to mini-HA. The sorted populations were analyzed by next-
328 generation sequencing. **(C)** Relationship between binding and expression scores. One data
329 point represents one light chain variant. Cyan: light chain variants from known IGHV1-69
330 antibodies to influenza virus. Blue: light chain variants from IGHV1-69 antibodies to non-
331 influenza antigens. Red: negative control variants with stop codons.

332

333 **Figure 2. Light chain sequence determinants for HA stem binding activity of CR9114. (A)**

334 Left panel: an extensive π - π stacking network at the heavy-light chain interface of CR9114 that
335 involves V_H W47, V_H Y98, V_H Y99, V_H Y100, V_H Y100a, and V_L W91. Right panel: Side chains of
336 V_L W91, A96 and F98 at the heavy-light chain interface of CR9114, with heavy chain in surface
337 representation. PDB 4FQI is used.⁷ Light blue: heavy chain; pink: light chain. V_H and V_L indicate
338 variable regions of antibody heavy and light chains, respectively. **(B)** Sequence logos for V_L
339 residues 91 and 96 of light chain variants with binding scores >0.8 (left panel) and <0.8 (right
340 panel). Relative sizes of the letters indicate their frequency among the variants. **(C)** Binding

341 scores of light chain variants in different IGLV families with and without $V_L 91_{F/Y/W}/96_{non-F/Y/W}$ are
342 compared. Red: with $V_L 91_{F/Y/W}/96_{non-F/Y/W}$; Blue: without $V_L 91_{F/Y/W}/96_{non-F/Y/W}$. P-values were
343 computed by two-tailed Student's t-test.

344

345 **Figure 3. Yeast display of CDR H3 library of CR9114 gHC. (A)** Schematic illustration of
346 measuring the expression level and HA stem binding activity of many CDR H3 variants in
347 parallel using yeast surface display. Briefly, a CDR H3 library of CR9114 gHC was displayed on
348 the yeast cell surface and subjected to FACS based on surface expression level and binding to
349 mini-HA. The sorted populations were analyzed by next-generation sequencing. **(B)**
350 Relationship between apparent dissociation constant (K_D) values and expression scores.
351 Greenish yellow: CR9114 single amino acid mutants; purple: nonsense variants with stop
352 codons; red: CDR H3 variants from IGHV1-69 HA stem antibodies; orange: CDR H3 variants
353 from IGHV1-69 non-HA stem influenza antibodies; grey: CDR H3 variants from IGHV1-69 non-
354 influenza antibodies; pink: WT. The Pearson correlation coefficient (R) is indicated. **(C)**
355 Distribution of the apparent K_D values among CDR H3 variants from different types of antibodies.
356 **(D)** Comparison of apparent K_D values between antibodies with and without $V_H Y98$. **(E)**
357 Comparison of apparent K_D values between antibodies with and without a Tyr in their CDR H3.
358 P-values were computed by two-tailed Student's t-test.

359

360 **Figure 4. Importance of $V_H H95$ and $N97$ for HA stem binding activity of CR9114. (A)**
361 Apparent K_D values of individual mutations in the CDR H3 of CR9114 are shown as a heatmap.
362 Wild-type (WT) amino acids are indicated by a black circle. **(B)** Intramolecular interactions
363 involving CR9114 $V_H H95$ are shown. **(C)** Intramolecular Interactions involving CR9114 $V_H N97$
364 are shown. Hydrogen bonds are represented by dashed lines. PDB 4FQI is used.⁷

365

366 **METHODS**

367 **CR9114 gHC yeast display plasmid**

368 CR9114 gHC yeast display plasmid, pCTcon2_CR9114_GL, was generated by cloning the
369 coding sequences of (from N-terminal to C-terminal, all in-frame) Aga2 secretion signal,
370 CR9114 wild-type Fab light chain, V5 tag, equine rhinitis B virus (ERBV-1) 2A self-cleaving
371 peptide, Aga2 secretion signal, CR9114 germline Fab heavy chain, HA tag, and Aga2p, into the
372 pCTcon2 vector.²⁶

373

374 **Construction of CDR H3 library and light chain variant library**

375 Sequences of IGHV1-69 antibodies were obtained from GenBank
376 (<https://www.ncbi.nlm.nih.gov/genbank/>).²⁷ IgBLAST was used to identify the CDR H3 region.²⁸
377 Light chain variant library (**Table S1**) and CDR H3 library (**Table S2**) were synthesized as oligo
378 pools by Integrated DNA Technologies and Twist Bioscience, respectively. Names and
379 sequences of primers for cloning the libraries into pCTcon2_CR9114_GL are listed in **Table S3**.
380 Oligo pool of the light chain variant library was PCR-amplified using primers IGHV1-69-
381 Lightchain-lib-IF and IGHV1-69-Lightchain-lib-IR. Then, the amplified oligonucleotide pool was
382 gel-purified using a Monarch DNA Gel Extraction Kit (NEB). To generate the linearized vector
383 for the light chain variant library, pCTcon2_CR9114_GL was used as a template for PCR using
384 primers IGHV1-69-Lightchain-lib-VF and IGHV1-69-Lightchain-lib-VR. The PCR product was
385 then gel-purified. Similarly, oligo pool of the CDR H3 library was PCR-amplified using primers
386 IGHV1-69-CDRH3-lib-IF and IGHV1-69-CDRH3-lib-IR. Then, the amplified oligo pool was gel-
387 purified using a Monarch DNA Gel Extraction Kit (NEB). To generate the linearized vector for
388 the light chain variant library, pCTcon2_ CR9114_GL was used as a template for PCR using
389 primers IGHV1-69-CDRH3-lib-VF and IGHV1-69-CDRH3-lib-VR. The PCR product was then
390 gel-purified. All PCRs were performed using KOD Hot Start DNA polymerase (EMD Millipore)
391 according to the manufacturer's instructions.

392

393 **Yeast transformation**

394 Yeast cells were transformed by electroporation following a previously described
395 protocol.²⁹ Briefly, *Saccharomyces cerevisiae* EBY100 cells (American Type Culture Collection)
396 were grown in YPD medium (1% w/v yeast nitrogen base, 2% w/v peptone, 2% w/v D(+)-
397 glucose) overnight at 30°C with shaking at 225 rpm until OD₆₀₀ reached 3. Then, an aliquot of
398 overnight culture was grown in 100 mL YPD media, with an initial OD₆₀₀ of 0.3, shaking at
399 225 rpm at 30°C. Once OD₆₀₀ reached 1.6, yeast cells were collected by centrifugation at
400 1700 × g for 3 min at room temperature. Media were removed and the cell pellet was
401 washed twice with 50 mL ice-cold water, and then once with 50 mL of ice-cold electroporation
402 buffer (1 M sorbitol, 1 mM calcium chloride). Cells were resuspended in 20 mL conditioning
403 media (0.1 M lithium acetate, 10 mM dithiothreitol) and shaken at 225 rpm at 30°C. Cells
404 were collected via centrifugation at 1700 × g for 3 min at room temperature, washed once
405 with 50 mL ice-cold electroporation buffer, resuspended in electroporation buffer to reach a
406 final volume of 1 mL, and kept on ice. 5 µg of the amplified oligo pool (light chain variant
407 library or CDR H3 library) and 4 µg of the corresponding purified linearized vector were added
408 into 400 µL of conditioned yeast. The mixture was transferred to a pre-chilled BioRad
409 GenePulser cuvette with 2 mm electrode gap and kept on ice for 5 min until electroporation.
410 Cells were electroporated at 2.5 kV and 25 µF, achieving a time constant between 3.7 and
411 4.1 ms. Electroporated cells were transferred into 4 mL of YPD media supplemented with
412 4 mL of 1 M sorbitol and incubated at 30°C with shaking at 225 rpm for 1 h. Cells were
413 collected via centrifugation at 1700 × g for 3 min at room temperature, resuspended in
414 0.6 mL SD-CAA medium (2% w/v D-glucose, 0.67% w/v yeast nitrogen base with ammonium
415 sulfate, 0.5% w/v casamino acids, 0.54% w/v Na₂HPO₄, 0.86% w/v NaH₂PO₄·H₂O, all dissolved
416 in deionized water), plated onto SD-CAA plates (2% w/v D-glucose, 0.67% w/v yeast nitrogen
417 base with ammonium sulfate, 0.5% w/v casamino acids, 0.54% w/v Na₂HPO₄, 0.86% w/v
418 NaH₂PO₄·H₂O, 18.2% w/v sorbitol, 1.5% w/v agar, all dissolved in deionized water) and

419 incubated at 30°C for 40 h. Colonies were then collected in SD-CAA medium, centrifuged at
420 1700 × g for 5 min at room temperature, and resuspended in SD-CAA medium with 15% v/v
421 glycerol such that OD₆₀₀ was 50. Glycerol stocks were stored at -80°C until used.

422

423 **Expression and purification of mini-HA**

424 The mini-HA #4900 protein⁵ was fused with N-terminal gp67 signal peptide and a C-terminal
425 BirA biotinylation site, thrombin cleavage site, trimerization domain, and a His₆ tag, and then
426 cloned into a customized baculovirus transfer vector³⁰. Recombinant bacmid DNA that carried
427 the mini-HA domain was generated using the Bac-to-Bac system (Thermo Fisher Scientific)
428 according to the manufacturer's instructions. Baculovirus was generated by transfecting the
429 purified bacmid DNA into adherent Sf9 cells using Cellfectin reagent (Thermo Fisher Scientific)
430 according to the manufacturer's instructions. The baculovirus was further amplified by
431 passaging in adherent Sf9 cells at a multiplicity of infection (MOI) of 1. Recombinant mini-HA
432 protein was expressed by infecting 1 L of suspension Sf9 cells at an MOI of 1. On day 3 post-
433 infection, Sf9 cells were pelleted by centrifugation at 4000 × g for 25 min, and soluble
434 recombinant mini-HA was purified from the supernatant by affinity chromatography using Ni
435 Sepharose excel resin (Cytiva) and then size exclusion chromatography using a HiLoad 16/100
436 Superdex 200 prep grade column (Cytiva) in 20 mM Tris-HCl pH 8.0, 100 mM NaCl. The
437 purified mini-HA protein was concentrated by Amicon spin filter (Millipore Sigma) and filtered by
438 0.22 μm centrifuge Tube Filters (Costar). Concentration of the protein was determined by
439 nanodrop (Fisher Scientific). Protein was subsequent aliquoted, flash frozen by dry-ice ethanol
440 mixture, and store at -80°C until used.

441

442 **Biotinylation and PE-conjugation of mini-HA**

443 Purified mini-HA was biotinylated using the Biotin-Protein Ligase-BIRA kit according to the
444 manufacturer's instructions (Avidity). Biotinylated mini-HA was then conjugated to streptavidin-
445 PE (Thermo Fisher Scientific) by incubating at room temperature for 15 mins.

446

447 **Fluorescence-activated cell sorting (FACS) of yeast display library**

448 100 μ L glycerol stock of the yeast display library was recovered in 50 mL SD-CAA medium by
449 incubating at 27 $^{\circ}$ C with shaking at 250 rpm until OD₆₀₀ reached between 1.5 and 2.0. Then
450 15 mL of the yeast culture was harvested and pelleted via centrifugation at 4000 \times g at 4 $^{\circ}$ C
451 for 5 min. The supernatant was discarded, and SGR-CAA (2% w/v galactose, 2% w/v raffinose,
452 0.1% w/v D-glucose, 0.67% w/v yeast nitrogen base with ammonium sulfate, 0.5% w/v
453 casamino acids, 0.54% w/v Na₂HPO₄, 0.86% w/v NaH₂PO₄·H₂O, all dissolved in deionized
454 water) was added to make up the volume to 50 mL. The yeast culture was then transferred to a
455 baffled flask and incubated at 18 $^{\circ}$ C with shaking at 250 rpm. Once OD₆₀₀ reached between
456 1.3 and 1.6, 1 mL of yeast culture was harvested and pelleted via centrifugation at
457 4000 \times g at 4 $^{\circ}$ C for 5 min. The pellet was subsequently washed with 1 mL of 1 \times PBS
458 twice. After the final wash, cells were resuspended in 1 mL of 1 \times PBS.

459

460 For expression sort, PE anti-HA.11 (epitope 16B12, BioLegend, Cat. No. 901517) that was
461 buffer-exchanged into 1 \times PBS was added to the cells at a final concentration of 1 μ g/mL. For
462 binding sort of the light chain variant library, PE-conjugated mini-HA was added to washed cells
463 at a final concentration of 30 nM. For Tite-Seq, cells were labeled with PE-conjugated mini-HA
464 at each of five antigen concentrations (one-log increments spanning 0.003 nM to 30 nM). A
465 negative control was set up with nothing added to the PBS-resuspended cells. Samples were
466 incubated overnight at 4 $^{\circ}$ C with rotation. Then, the yeast pellet was washed twice in 1 \times PBS
467 and resuspended in FACS tubes containing 2 mL 1 \times PBS. Using a BD FACS Aria II cell sorter
468 (BD Biosciences) and FACS Diva software v8.0.1 (BD Biosciences), cells in the selected gates

469 were collected in 1 mL of SD-CAA containing 1x penicillin/streptomycin. Single yeast cells
470 were gated by forward scatter (FSC) and side scatter (SSC). Single cells were then gated by PE
471 anti-HA.11 for expression sort. For Tite-Seq, single cells were gated into three bins along the
472 PE-A axis based on unstained and CR9114 gHC controls, with bin 0 comprising all PE negative
473 cells, bin 2 comprising PE positive cells with comparable expression or binding affinity to the
474 germline CR9114 positive population, and bin 1 comprising the intermediate population between
475 bin 0 and bin 2. Cells were then collected via centrifugation at 3800xg at 20°C for 15 min.
476 The supernatant was discarded. Subsequently, the pellet was resuspended in 100 µL of SD-
477 CAA and plated on SD-CAA plates at 30°C. After 40 h, colonies were collected in 2 mL of
478 SD-CAA. Frozen stocks were made by reconstituting the pellet in 15% v/v glycerol (in SD-CAA
479 medium) and then stored at -80°C until used. FlowJo v10.8 software (BD Life Sciences) was
480 used to analyze FACS data.

481

482 **Next-generation sequencing of light chain variant library and CDR H3 library**

483 Plasmids from the yeast cells were extracted using a Zymoprep Yeast Plasmid Miniprep II Kit
484 (Zymo Research) following the manufacturer's protocol. The CDR H3 library was subsequently
485 amplified by PCR using primers IGHV1-69-CDRH3-recover-F and IGHV1-69-CDRH3-recover-R
486 whereas the light chain variant library was amplified using primers IGHV1-69-Lightchain-
487 recover-F and IGHV1-69-Lightchain-R. Subsequently, adapters containing sequencing
488 barcodes were appended to the amplicon using primers 5'-AAT GAT ACG GCG ACC ACC GAG
489 ATC TAC ACX XXX XXX XAC ACT CTT TCC CTA CAC GAC GCT-3', and 5'-CAA GCA GAA
490 GAC GGC ATA CGA GAT XXX XXX XXG TGA CTG GAG TTC AGA CGT GTG CT-3'.
491 Positions annotated by an "X" represented the nucleotides for the index sequence. All PCRs
492 were performed using Q5 High-Fidelity DNA polymerase (NEB) according to the manufacturer's
493 instructions. PCR products were purified using PureLink PCR Purification Kit (Thermo Fisher

494 Scientific). The final PCR products were submitted for next generation sequencing using
495 NovaSeq SP PE250 (Illumina).

496

497 **Computing the binding score, expression score, and apparent K_D values**

498 The sequencing data was initially obtained in FASTQ format and subsequently analyzed using a
499 custom python Snakemake pipeline.³¹ Briefly, PEAR was used for merging the forward and
500 reverse reads.³² The number of reads corresponding to each variant in each sample is counted.
501 A pseudocount of 1 was added to the final count to avoid division by zero in downstream
502 analysis. The binding and expression enrichment values of each variant var were computed as
503 follows:

$$enrichment(var) = \log_{10} \frac{Count_{PE+}(var)}{Count_{PE-}(var)}$$

504 where the $Count_{PE+}(var)$ is the read count of variant var in the PE positive sample for a given
505 binding or expression sort, while $Count_{PE-}(var)$ is the read count of variant var in the PE
506 negative sample. The binding and expression scores for each variant var were further
507 computed from the enrichment values as follows:

$$score(var) = \frac{enrichment(var) - \overline{enrichment_{-ve\ control}}}{enrichment_{WT} - \overline{enrichment_{-ve\ control}}}$$

508 where $\overline{enrichment_{-ve\ control}}$ is the average enrichment value of the negative controls with stop
509 codons and $enrichment_{WT}$ is the enrichment value of the WT. The final score for each variant
510 var is the average of two biological replicates.

511

512 To compute apparent K_D value of each CDR H3 variant from the Tite-Seq data, we adopted the
513 analysis approach as previously described.³³ Briefly, to determine the mean bin of PE
514 fluorescence for each CDR H3 variant var at each mini-HA concentration, a simple weighted
515 mean calculation was applied:

$$\overline{Bin}_{[HA]}(var) = \left(\sum_{i=0}^2 N_{i,[HA]}(var) * (i + 1) \right) / \left(\sum_{i=0}^2 N_{i,[HA]}(var) \right)$$

516 where $N_{i,[HA]}(var)$ is the number of cells with CDR H3 variant var that fall into bin i at mini-HA
517 concentration $[HA]$. This calculation computes a weighted average by assigning integer weight
518 to the bin i .

519

520 For each CDR H3 variant var , we estimated its sorted cell count $N_{i,[HA]}(var)$ that corresponds
521 to bin i at mini-HA concentration $[HA]$ as follows:

$$N_{i,[HA]}(var) = Ntotal_{i,[HA]} \times \frac{C_{i,[HA]}(var)}{Ctotal_{i,[HA]}}$$

522 where variant read count $C_{i,[HA]}(var)$ is the read counts for CDR H3 variant var in bin i at mini-
523 HA concentration $[HA]$, $Ctotal_{i,[HA]}$ is the total read counts for bin i at mini-HA concentration
524 $[HA]$, $Ntotal_{i,[HA]}$ is the total number of cells in bin i at mini-HA concentration $[HA]$.

525

526 We then determined the apparent K_D value for each variant $K_D(var)$ HA via a nonlinear least-
527 squares regression using a standard non-cooperative Hill equation:

$$\overline{Bin}_{[HA]}(var) = a \times \frac{[HA]}{(K_D(var) + [HA])} + b$$

528 where free parameters a is titration response range and b is titration curve baseline.

529

530 CDR H3 variants with a total cell counts of less than 30 across bins 0 to 2 were discarded from
531 our analysis. CDR H3 variants with an apparent KD value $<10^{-8}$ and a p-value >0.2 were also
532 discarded. Light chain variants with an average occurrence frequency $\leq 0.2\%$ across different
533 sorted populations were discarded from our analysis. Sequence logos were generated by
534 Logomaker in Python.³⁴

535

536 **Expression and purification of Fabs**

537 The heavy and light chains of Fab were cloned into pHCMV3 vector. Light chain mutants were
538 generated using the QuikChange XL Mutagenesis kit (Stratagene) following the manufacturer's
539 instructions. The plasmids were co-transfected into Expi293F cells at a 2:1 (HC:LC) mass ratio
540 using ExpiFectamine 293 Reagent (Thermo Fisher Scientific). At 7 days post-transfection, the
541 supernatant was collected, and the Fab was purified using a CaptureSelect CH1-XL Pre-packed
542 Column (Thermo Fisher Scientific).

543

544 **Biolayer interferometry binding assay**

545 Binding assays were performed by biolayer interferometry (BLI) using an Octet Red96e
546 instrument (FortéBio) at room temperature as described previously.³⁵ Briefly, His-tagged mini-
547 HA proteins at 0.5 μ M in 1x kinetics buffer (1x PBS, pH 7.4, 0.01% w/v BSA and 0.002% v/v
548 Tween 20) were loaded onto anti-Penta-HIS (HIS1K) biosensors and incubated with the
549 indicated concentrations of Fabs. The assay consisted of five steps: (1) baseline: 60 s with 1x
550 kinetics buffer; (2) loading: 60 s with His-tagged mini-HA proteins; (3) baseline: 60 s with 1x
551 kinetics buffer; (4) association: 60 s with Fab samples; and (5) dissociation: 60 s with 1x
552 kinetics buffer. For estimating the exact K_D , a 1:1 binding model was used.

553

554 **Data availability**

555 Raw sequencing data have been submitted to the NIH Short Read Archive under BioProject:
556 PRJNA976657.

557

558 **Code availability**

559 Custom python scripts for all analyses have been deposited to:

560 https://github.com/nicwulab/CR9114_LC_CDRH3_screen

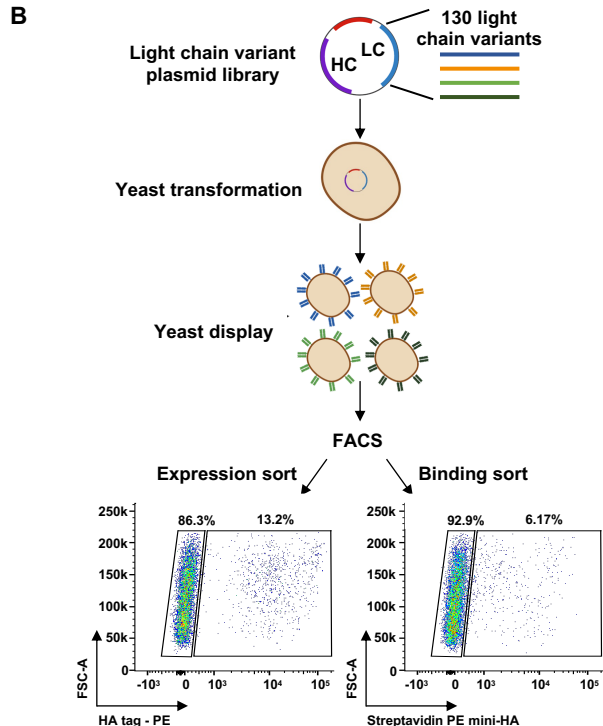
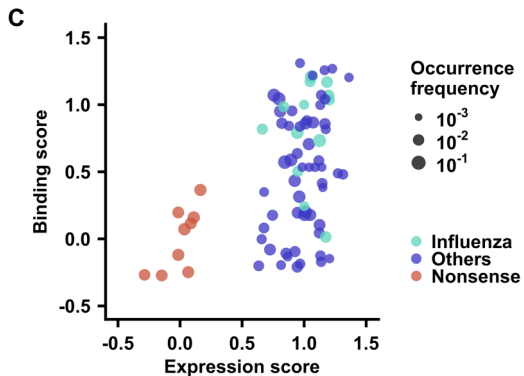
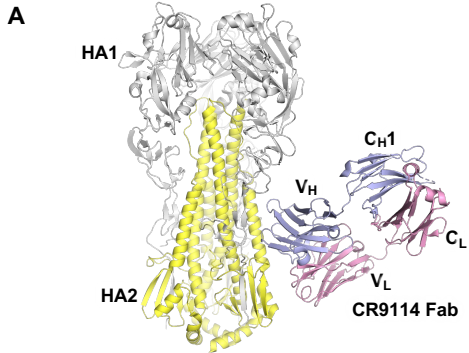
561

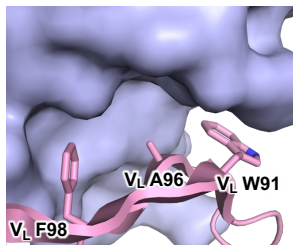
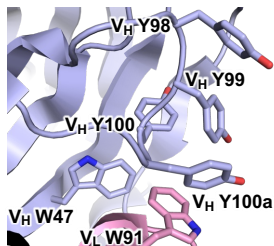
562 REFERENCES

- 563 1. Petrova, V.N., and Russell, C.A. (2018). The evolution of seasonal influenza viruses. *Nature*
564 *Reviews Microbiology* 16, 47-60.
- 565 2. Frentzel, E., Jump, R.L., Archbald-Pannone, L., Nace, D.A., Schweon, S.J., Gaur, S., Naqvi,
566 F., Pandya, N., and Mercer, W. (2020). Recommendations for mandatory influenza
567 vaccinations for health care personnel from AMDA's Infection Advisory Subcommittee.
568 *Journal of the American Medical Directors Association* 21, 25-28.e22.
- 569 3. Tricco, A.C., Chit, A., Soobiah, C., Hallett, D., Meier, G., Chen, M.H., Tashkandi, M., Bauch,
570 C.T., and Loeb, M. (2013). Comparing influenza vaccine efficacy against mismatched and
571 matched strains: a systematic review and meta-analysis. *BMC Medicine* 11, 1-19.
- 572 4. Carrat, F., and Flahault, A. (2007). Influenza vaccine: the challenge of antigenic drift.
573 *Vaccine* 25, 6852-6862.
- 574 5. Impagliazzo, A., Milder, F., Kuipers, H., Wagner, M.V., Zhu, X., Hoffman, R.M., van
575 Meersbergen, R., Huizingh, J., Wanningen, P., and Verspuij, J. (2015). A stable trimeric
576 influenza hemagglutinin stem as a broadly protective immunogen. *Science* 349, 1301-1306.
- 577 6. Yassine, H.M., Boyington, J.C., McTamney, P.M., Wei, C.-J., Kanekiyo, M., Kong, W.-P.,
578 Gallagher, J.R., Wang, L., Zhang, Y., and Joyce, M.G. (2015). Hemagglutinin-stem
579 nanoparticles generate heterosubtypic influenza protection. *Nature Medicine* 21, 1065-1070.
- 580 7. Dreyfus, C., Laursen, N.S., Kwaks, T., Zuijdgeest, D., Khayat, R., Ekiert, D.C., Lee, J.H.,
581 Metlagel, Z., Bujny, M.V., and Jongeneelen, M. (2012). Highly conserved protective
582 epitopes on influenza B viruses. *Science* 337, 1343-1348.
- 583 8. Andrews, S.F., Graham, B.S., Mascola, J.R., and McDermott, A.B. (2018). Is it possible to
584 develop a "universal" influenza virus vaccine? Immunogenetic considerations underlying B-
585 cell biology in the development of a pan-subtype influenza A vaccine targeting the
586 hemagglutinin stem. *Cold Spring Harbor Perspectives in Biology* 10, a029413.
- 587 9. Throsby, M., van den Brink, E., Jongeneelen, M., Poon, L.L., Alard, P., Cornelissen, L.,
588 Bakker, A., Cox, F., van Deventer, E., and Guan, Y. (2008). Heterosubtypic neutralizing
589 monoclonal antibodies cross-protective against H5N1 and H1N1 recovered from human
590 IgM+ memory B cells. *PLOS One* 3, e3942.
- 591 10. Pappas, L., Foglierini, M., Piccoli, L., Kallewaard, N.L., Turrini, F., Silacci, C., Fernandez-
592 Rodriguez, B., Agatic, G., Giacchetto-Sasselli, I., and Pellicciotta, G. (2014). Rapid
593 development of broadly influenza neutralizing antibodies through redundant mutations.
594 *Nature* 516, 418-422.
- 595 11. Sui, J., Hwang, W.C., Perez, S., Wei, G., Aird, D., Chen, L.-m., Santelli, E., Stec, B.,
596 Cadwell, G., and Ali, M. (2009). Structural and functional bases for broad-spectrum
597 neutralization of avian and human influenza A viruses. *Nature Structural & Molecular*
598 *Biology* 16, 265-273.

- 599 12. Ekiert, D.C., Bhabha, G., Elsliger, M.-A., Friesen, R.H., Jongeneelen, M., Throsby, M.,
600 Goudsmit, J., and Wilson, I.A. (2009). Antibody recognition of a highly conserved influenza
601 virus epitope. *Science* 324, 246-251.
- 602 13. Lang, S., Xie, J., Zhu, X., Wu, N.C., Lerner, R.A., and Wilson, I.A. (2017). Antibody 27F3
603 broadly targets influenza A group 1 and 2 hemagglutinins through a further variation in V_H1-
604 69 antibody orientation on the HA stem. *Cell Reports* 20, 2935-2943.
- 605 14. Avnir, Y., Tallarico, A.S., Zhu, Q., Bennett, A.S., Connelly, G., Sheehan, J., Sui, J., Fahmy,
606 A., Huang, C.-y., and Cadwell, G. (2014). Molecular signatures of hemagglutinin stem-
607 directed heterosubtypic human neutralizing antibodies against influenza A viruses. *PLoS*
608 *Pathogens* 10, e1004103.
- 609 15. Chen, F., Tzarum, N., Wilson, I.A., and Law, M. (2019). V_H1-69 antiviral broadly neutralizing
610 antibodies: genetics, structures, and relevance to rational vaccine design. *Current Opinion*
611 *in Virology* 34, 149-159.
- 612 16. Xu, R., Krause, J.C., McBride, R., Paulson, J.C., Crowe Jr, J.E., and Wilson, I.A. (2013). A
613 recurring motif for antibody recognition of the receptor-binding site of influenza
614 hemagglutinin. *Nature Structural & Molecular Biology* 20, 363-370.
- 615 17. Lee, P.S., Ohshima, N., Stanfield, R.L., Yu, W., Iba, Y., Okuno, Y., Kurosawa, Y., and
616 Wilson, I.A. (2014). Receptor mimicry by antibody F045–092 facilitates universal binding to
617 the H3 subtype of influenza virus. *Nature Communications* 5, 3614.
- 618 18. Phillips, A.M., Lawrence, K.R., Moulana, A., Dupic, T., Chang, J., Johnson, M.S., Cvijovic, I.,
619 Mora, T., Walczak, A.M., and Desai, M.M. (2021). Binding affinity landscapes constrain the
620 evolution of broadly neutralizing anti-influenza antibodies. *eLife* 10, e71393.
- 621 19. Boyd, S.D., Gaëta, B.A., Jackson, K.J., Fire, A.Z., Marshall, E.L., Merker, J.D., Maniar, J.M.,
622 Zhang, L.N., Sahaf, B., and Jones, C.D. (2010). Individual variation in the germline Ig gene
623 repertoire inferred from variable region gene rearrangements. *The Journal of Immunology*
624 184, 6986-6992.
- 625 20. Lerner, R.A. (2011). Rare antibodies from combinatorial libraries suggests an SOS
626 component of the human immunological repertoire. *Molecular BioSystems* 7, 1004-1012.
- 627 21. Erbeling, E.J., Post, D.J., Stemmy, E.J., Roberts, P.C., Augustine, A.D., Ferguson, S.,
628 Paules, C.I., Graham, B.S., and Fauci, A.S. (2018). A universal influenza vaccine: the
629 strategic plan for the National Institute of Allergy and Infectious Diseases. *The Journal of*
630 *Infectious Diseases* 218, 347-354.
- 631 22. Nachbagauer, R., Feser, J., Naficy, A., Bernstein, D.I., Guptill, J., Walter, E.B., Berlanda-
632 Scorza, F., Stadlbauer, D., Wilson, P.C., and Aydiillo, T. (2021). A chimeric hemagglutinin-
633 based universal influenza virus vaccine approach induces broad and long-lasting immunity
634 in a randomized, placebo-controlled phase I trial. *Nature Medicine* 27, 106-114.
- 635 23. Andrews, S.F., Cominsky, L.Y., Shimberg, G.D., Gillespie, R.A., Gorman, J., Raab, J.E.,
636 Brand, J., Creanga, A., Gajjala, S.R., and Narpala, S. (2023). An influenza H1
637 hemagglutinin stem-only immunogen elicits a broadly cross-reactive B cell response in
638 humans. *Science Translational Medicine* 15, eade4976.

- 639 24. Adams, R.M., Mora, T., Walczak, A.M., and Kinney, J.B. (2016). Measuring the sequence-
640 affinity landscape of antibodies with massively parallel titration curves. *eLife* 5, e23156.
- 641 25. Starr, T.N., Greaney, A.J., Hilton, S.K., Ellis, D., Crawford, K.H., Dings, A.S., Navarro,
642 M.J., Bowen, J.E., Tortorici, M.A., and Walls, A.C. (2020). Deep mutational scanning of
643 SARS-CoV-2 receptor binding domain reveals constraints on folding and ACE2 binding.
644 *Cell* 182, 1295-1310.e1220.
- 645 26. Chao, G., Lau, W.L., Hackel, B.J., Sazinsky, S.L., Lippow, S.M., and Wittrup, K.D. (2006).
646 Isolating and engineering human antibodies using yeast surface display. *Nature Protocols* 1,
647 755-768.
- 648 27. Benson, D.A., Cavanaugh, M., Clark, K., Karsch-Mizrachi, I., Lipman, D.J., Ostell, J., and
649 Sayers, E.W. (2012). GenBank. *Nucleic Acids Research* 41, D36-D42.
- 650 28. Ye, J., Ma, N., Madden, T.L., and Ostell, J.M. (2013). IgBLAST: an immunoglobulin variable
651 domain sequence analysis tool. *Nucleic Acids Research* 41, W34-W40.
- 652 29. Benatuil, L., Perez, J.M., Belk, J., and Hsieh, C.-M. (2010). An improved yeast
653 transformation method for the generation of very large human antibody libraries. *Protein*
654 *Engineering, Design and Selection* 23, 155-159.
- 655 30. Ekiert, D.C., Friesen, R.H., Bhabha, G., Kwaks, T., Jongeneelen, M., Yu, W., Ophorst, C.,
656 Cox, F., Korse, H.J., and Brandenburg, B. (2011). A highly conserved neutralizing epitope
657 on group 2 influenza A viruses. *Science* 333, 843-850.
- 658 31. Mölder, F., Jablonski, K.P., Letcher, B., Hall, M.B., Tomkins-Tinch, C.H., Sochat, V., Forster,
659 J., Lee, S., Twardziok, S.O., and Kanitz, A. (2021). Sustainable data analysis with
660 Snakemake. *F1000Research* 10.
- 661 32. Zhang, J., Kobert, K., Flouri, T., and Stamatakis, A. (2014). PEAR: a fast and accurate
662 Illumina Paired-End reAd mergeR. *Bioinformatics* 30, 614-620.
- 663 33. Starr, T.N., Greaney, A.J., Hilton, S.K., Ellis, D., Crawford, K.H., Dings, A.S., Navarro,
664 M.J., Bowen, J.E., Tortorici, M.A., and Walls, A.C. (2020). Deep mutational scanning of
665 SARS-CoV-2 receptor binding domain reveals constraints on folding and ACE2 binding.
666 *Cell* 182, 1295-1310. e1220.
- 667 34. Tareen, A., and Kinney, J.B. (2020). Logomaker: beautiful sequence logos in Python.
668 *Bioinformatics* 36, 2272-2274.
- 669 35. Wu, N.C., Grande, G., Turner, H.L., Ward, A.B., Xie, J., Lerner, R.A., and Wilson, I.A.
670 (2017). In vitro evolution of an influenza broadly neutralizing antibody is modulated by
671 hemagglutinin receptor specificity. *Nature Communications* 8, 15371.
672

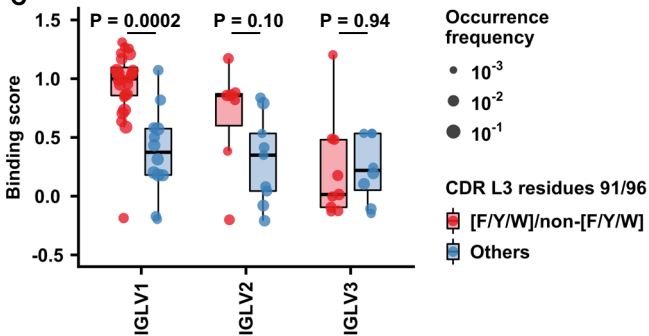


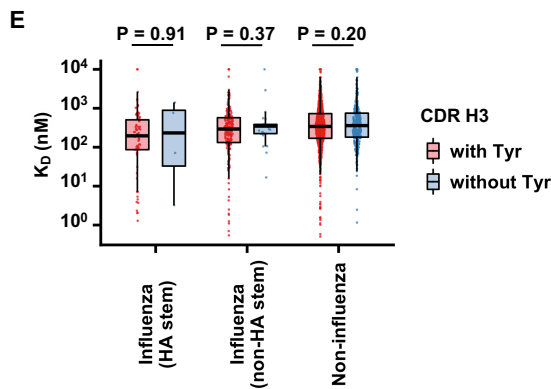
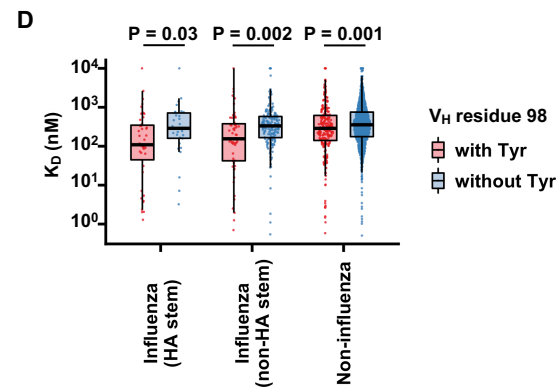
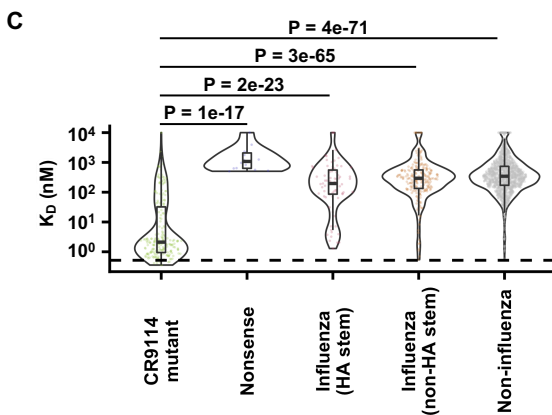
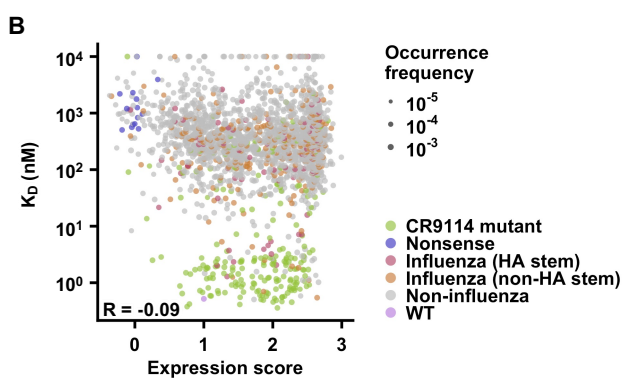
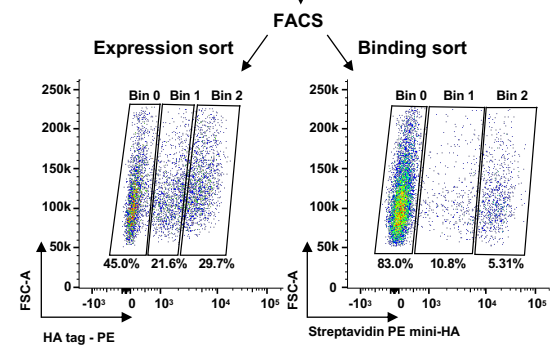
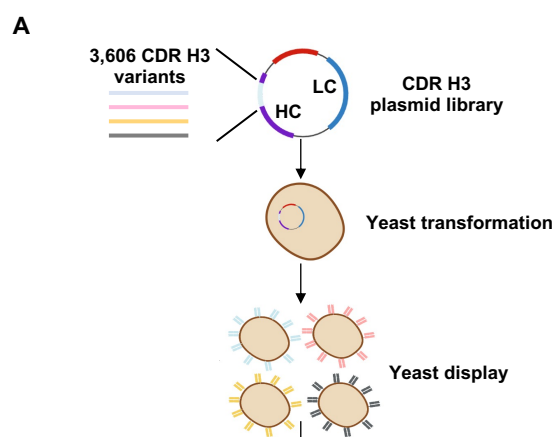
A**B**

Binding score > 0.8
(n = 28)



Binding score < 0.8
(n = 41)

**C**



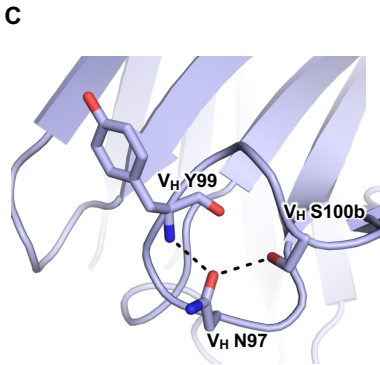
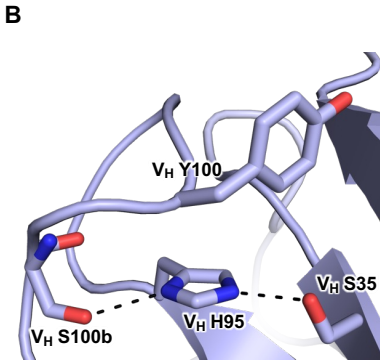
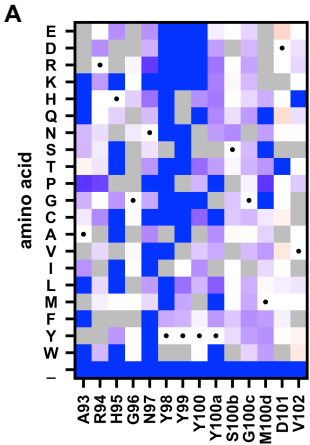
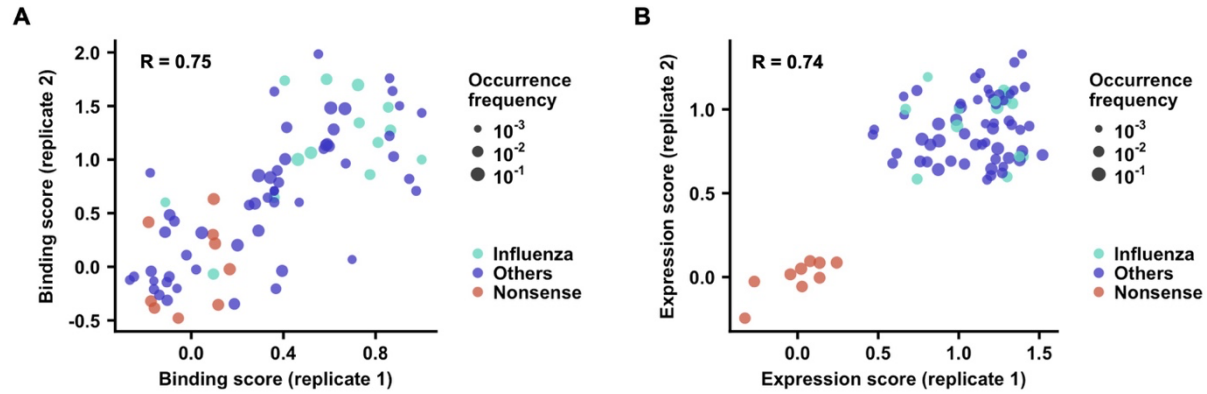
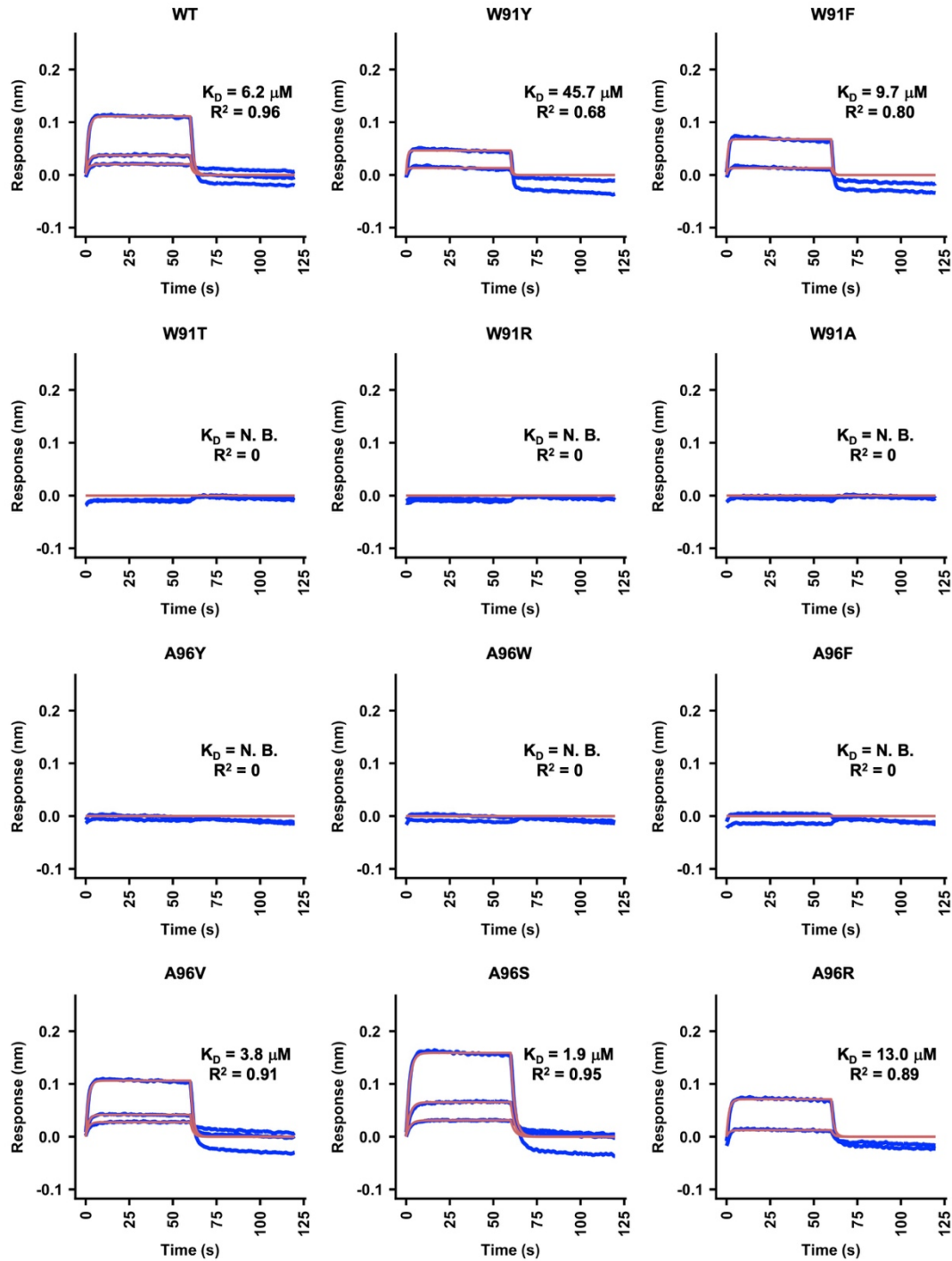


Table 1. Binding affinity of CR9114 gHC mutants against mini-HA. N.B. indicates no binding.

CR9114 gHC mutant Fab	K_D (μM)
WT	6.2
V _L W91Y	45.7
V _L W91F	9.7
V _L W91T	N.B.
V _L W91R	N.B.
V _L W91A	N.B.
V _L A96Y	N.B.
V _L A96W	N.B.
V _L A96F	N.B.
V _L A96V	3.8
V _L A96S	1.9
V _L A96R	13.0



Supplementary Figure 1. Correlation between biological replicates of binding and expression sorts of CR9114 light chain variant library. (A) Correlation of binding scores between two independent biological replicates is shown. **(B)** Correlation of expression scores between two independent biological replicates is shown. Cyan: light chain variants from known IGHV1-69 antibodies to influenza virus. Blue: light chain variants from IGHV1-69 antibodies to non-influenza antigens. Red: negative control variants with premature stop codons. The Pearson correlation coefficient (R) is indicated.

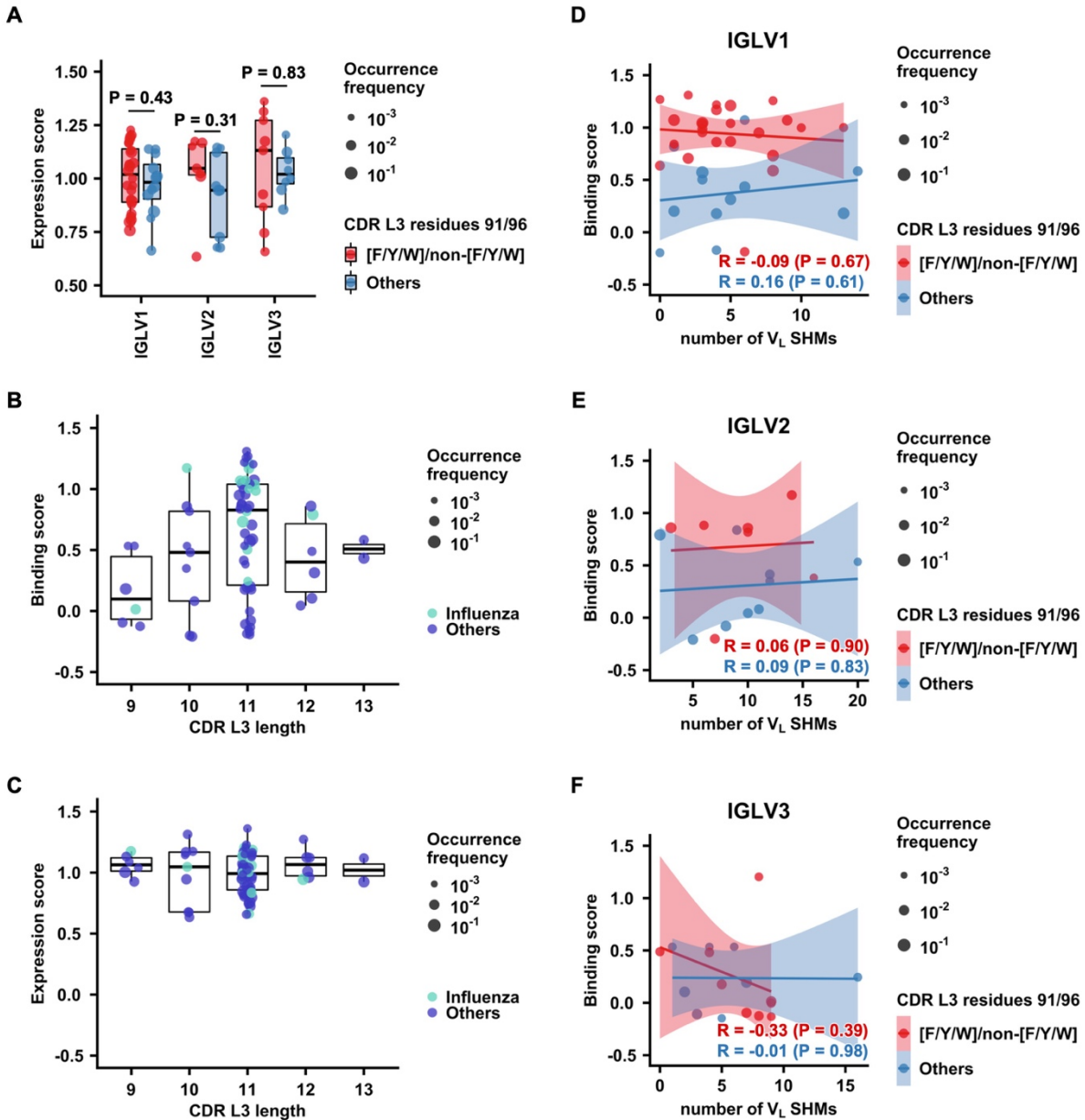


Supplementary Figure 2. Sensorgrams for binding of CR9114 gHC mutants to mini-HA. (A)

Binding kinetics of different Fabs against mini-HA were measured by biolayer interferometry (BLI).

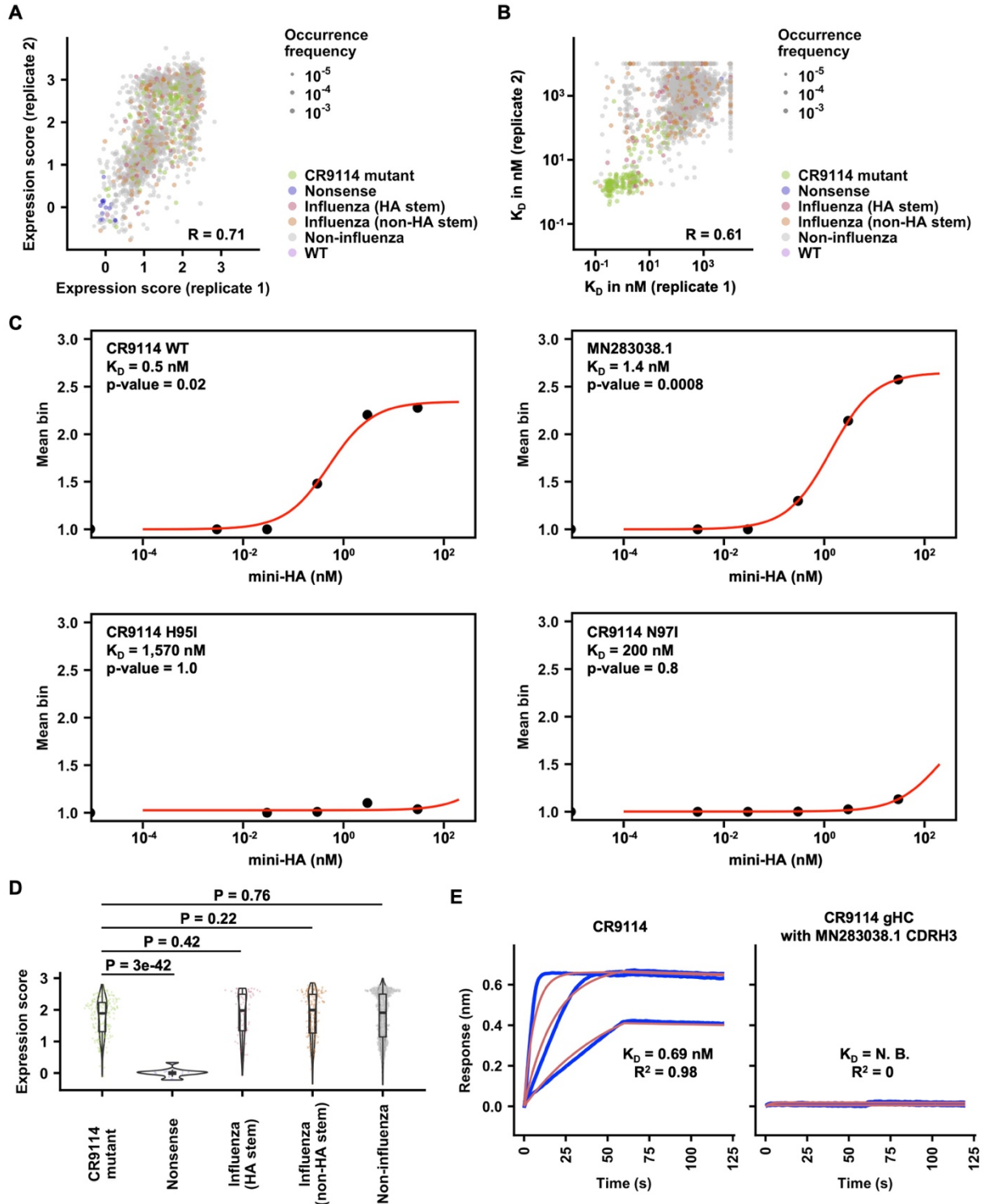
Y-axis represents the response. Blue lines represent the response curve and red lines represent

a 1:1 binding model. Binding kinetics were measured for two to three Fab concentrations. N.B. indicates no binding. Dissociation constant (K_D) and the goodness of model fitting (R^2) are indicated.



Supplementary Figure 3. Impact of CDR L3 length and somatic hypermutation (SHM) on HA stem binding activity of CR9114. (A) Expression scores of light chain variants in different IGLV families with and without V_L 91_{F/Y/W}/96_{non-F/Y/W} are compared. Red: with V_L 91_{F/Y/W}/96_{non-F/Y/W}; Blue: without V_L 91_{F/Y/W}/96_{non-F/Y/W}. P-values were computed by two-tailed Student's t-test. **(B-C)** Binding **(B)** and expression **(C)** scores of light chain variants with different CDR L3 lengths are compared. Cyan: light chain variants from known IGHV1-69 antibodies to influenza virus. Blue:

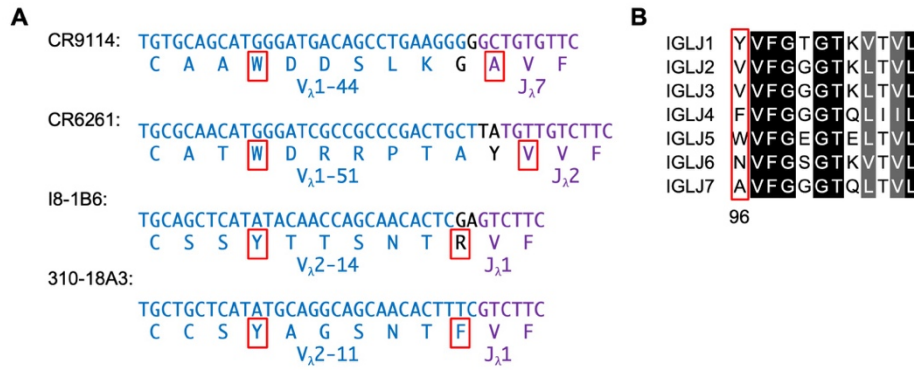
light chain variants from IGHV1-69 antibodies to non-influenza antigens. **(D-F)** Correlation between binding score and the number V_L SHM is shown for light chain variants in different light chain families, namely IGLV1 **(D)**, IGLV2 **(E)**, and IGLV3 **(F)**. The Pearson correlation coefficient **(R)** is indicated. P-values were computed by Pearson correlation test.



Supplementary Figure 4. Reproducibility and analysis of Tite-Seq for CDR H3 variants. (A)

Correlation of expression scores between two independent biological replicates is shown. (B)

Correlation of apparent dissociation constant (K_D) values between two independent biological replicates is shown. **(C)** Example titration curves inferred from Tite-Seq data. **(D)** Distributions of expression scores for CDR H3 variants from different types of antibodies. Greenish yellow: CR9114 single amino acid mutants; purple: nonsense variants with stop codons; red: CDR H3 variants from IGHV1-69 HA stem antibodies; orange: CDR H3 variants from IGHV1-69 non-HA stem influenza antibodies; grey: CDR H3 variants from IGHV1-69 non-influenza antibodies; pink: WT. **(E)** Binding kinetics of a CDR H3 variant from an IGHV1-69 non-influenza antibody (Genbank ID: MN283038.1) and CR9114 (positive control) to mini-HA were measured by BLI. Y-axis represents the response. Blue lines represent the response curve and red lines represent a 1:1 binding model. Binding kinetics were measured for at least two Fab concentrations. N.B. indicates no binding. Dissociation constant (K_D) and the goodness of model fitting (R^2) are indicated.



Supplementary Figure 5. V_L residue 96 is sometimes encoded by IGLJ. (A) Nucleotide and amino acid sequences of light chain V-J junction are shown for different IGHV1-69 HA stem antibodies. V_L residues 91 and 96 are indicated in red. Blue: V-region; purple: J-region; black: N-region. **(B)** CDR L3 sequences among different IGLJ families. V_L residue 96 is indicated in red.

Supplementary Table 3. List of primers used in this study.

Primer Name	Sequence (5' to 3')
V _H 1-69-Lightchain-lib-VF	GGACAACCAAAGGCTGCTCCTTC
V _H 1-69-LightChain-lib-VR	GGCCGGCTGGGCCGCTGCTAAACTGA
V _H 1-69-LightChain-lib-IF	TTTCAATATTTTCTGTTATTGCTTCAGTTTTAGCAGCGGCCAGCCGGCC
V _H 1-69-LightChain-lib-IR	TCAGAGGATGGAGGGAACAAGGTGACAGAAGGAGCAGCCTTTGGTTGTCC
V _H 1-69-LightChain-recover-F	CAGTTTTAGCAGCGGCCAGCCG
V _H 1-69-LightChain-recover-R	ACAGAAGGAGCAGCCTTTGGTTG
V _H 1-69-CDRH3-VF	GGCCAAGGGACCACGGTCACCGTCTCCTCAGCTTC
V _H 1-69-CDRH3-VR	GTAATACACGGCCGTGTCCTCAGATCTCAGGCTGC
V _H 1-69-CDRH3-lib-F	CACAGCCTACATGGAGCTGAGCAGCCTGAGATCTGAGGACACGGCCGTGATTAC
V _H 1-69-CDRH3-lib-R	AAAACGGAAGGTCCCTTAGTAGAAGCTGAGGAGACGGTGACCGTGGTCCCTTGGC
V _H 1-69-CDRH3-recover-F	ATCTGAGGACACGGCCGTGATTAC
V _H 1-69-CDRH3-recover-R	AGACGGTGACCGTGGTCCCTTGGCC